



## Article

# Monitoring Water Quality of the Haihe River Based on Ground-Based Hyperspectral Remote Sensing

Qi Cao <sup>1</sup> , Gongliang Yu <sup>2</sup> , Shengjie Sun <sup>1</sup>, Yong Dou <sup>1</sup>, Hua Li <sup>2</sup> and Zhiyi Qiao <sup>1,\*</sup>

<sup>1</sup> Tianjin Key Laboratory of Aqua-Ecology and Aquaculture, College of Fisheries, Tianjin Agricultural University, Tianjin 300384, China; 1904010103@stu.tjau.edu.cn (Q.C.); tjaisunsj@hotmail.com (S.S.); Douyonghero@163.com (Y.D.)

<sup>2</sup> CAS Key Laboratory of Algal Biology, Institute of Hydrobiology, Chinese Academy of Sciences, Wuhan 430072, China; yugl@ihb.ac.cn (G.Y.); lih@ihb.ac.cn (H.L.)

\* Correspondence: zhiyiqiao@tjau.edu.cn; Tel.: +86-022-23781299

**Abstract:** The Haihe River is a typical sluice-controlled river in the north of China. The construction and operation of sluice dams change the flow and other hydrological factors of rivers, which have adverse effects on water, making it difficult to study the characteristics of water quality change and water environment control in northern rivers. In recent years, remote sensing has been widely used in water quality monitoring. However, due to the low signal-to-noise ratio (SNR) and the limitation of instrument resolution, satellite remote sensing is still a challenge to inland water quality monitoring. Ground-based hyperspectral remote sensing has a high temporal-spatial resolution and can be simply fixed in the water edge to achieve real-time continuous detection. A combination of hyperspectral remote sensing devices and BP neural networks is used in the current research to invert water quality parameters. The measured values and remote sensing reflectance of eight water quality parameters (chlorophyll-a (Chl-a), phycocyanin (PC), total suspended sediments (TSS), total nitrogen (TN), total phosphorus (TP), ammonia nitrogen (NH<sub>4</sub>-N), nitrate-nitrogen (NO<sub>3</sub>-N), and pH) were modeled and verified. The results show that the performance R<sup>2</sup> of the training model is above 80%, and the performance R<sup>2</sup> of the verification model is above 70%. In the training model, the highest fitting degree is TN (R<sup>2</sup> = 1, RMSE = 0.0012 mg/L), and the lowest fitting degree is PC (R<sup>2</sup> = 0.87, RMSE = 0.0011 mg/L). Therefore, the application of hyperspectral remote sensing technology to water quality detection in the Haihe River is a feasible method. The model built in the hyperspectral remote sensing equipment can help decision-makers to easily understand the real-time changes of water quality parameters.

**Keywords:** ground-based remote sensing; hyperspectral; water quality; BP neural network; Haihe River



**Citation:** Cao, Q.; Yu, G.; Sun, S.; Dou, Y.; Li, H.; Qiao, Z. Monitoring Water Quality of the Haihe River Based on Ground-Based Hyperspectral Remote Sensing. *Water* **2022**, *14*, 22. <https://doi.org/10.3390/w14010022>

Academic Editors: Zheng Duan and Babak Mohammadi

Received: 3 November 2021

Accepted: 19 December 2021

Published: 22 December 2021

**Publisher's Note:** MDPI stays neutral with regard to jurisdictional claims in published maps and institutional affiliations.



**Copyright:** © 2021 by the authors. Licensee MDPI, Basel, Switzerland. This article is an open access article distributed under the terms and conditions of the Creative Commons Attribution (CC BY) license (<https://creativecommons.org/licenses/by/4.0/>).

## 1. Introduction

The lack of water resources is one of the most important global issues that human society is currently facing. Water resource security is one of the international research spotlights in recent years [1]. Monitoring water quality is an essential tool for determining and controlling pollution-prone areas to conserve drinking water safety [2]. Traditional monitoring methods of water quality variables are to select fixed sampling points, to collect samples regularly, and to bring the water samples back to the laboratory for analysis, which cannot provide the water quality data of the same period at the regional scale, and is generally a time-consuming and labor-intensive process [3,4]. It shows obvious limitations for continuous monitoring of fixed points. The YSI multi-parameter water quality analyzer is a commonly used portable multi-parameter water quality analyzer, which can detect several physical and chemical indicators of water in the field, but the price of the analyzer is relatively high. When different indicators are detected, the probe needs to be replaced and calibrated with a standard solution, otherwise, the accuracy of the data will be affected. The monitoring method of the buoy station is to place the water quality sensor on the

buoy and supply power through the solar charging plate and battery so that the water body in the area where the buoy station is located can be continuously monitored without anyone. However, the buoy will deviate from the placement position under the influence of wind, thus affecting the accuracy of data. The water undergoes continuous and dynamic changes, and therefore, continuous water quality monitoring is important as a method for determining hygienic conditions.

Since the 1980s, remote sensing has become a powerful tool for lake monitoring [5]. Spectral imaging takes advantage of the fact that each material has its unique spectral signature, and the spectrum of individual pixels in the image provides information about its composition and material surface [6]. Hyperspectral remote sensing combines the benefits from remote sensing and spectroscopy. In hyperspectral remote sensing, spectral data are usually high dimensional and fine spectral bands that are highly correlated with each other [7]. These spectral signatures support the identification of elements or the measurement of concentrations [8]. Therefore, hyperspectral remote sensing technology is more suitable for complex inland bodies of water with changeable optical characteristics. The substances in the water determine the spectral characteristics of the water body, and the substances affecting the spectral distribution and light intensity in the inland surface water can be roughly divided into three categories: phytoplankton pigments, yellow substances, and suspended substances [9]. Hyperspectral technology has been widely applied to water quality parameters with optical activity, such as Chl-a [10,11] PC [12,13], TSS [14,15], chromophoric dissolved organic matter (CDOM) [16], transparency [17], and turbidity [18]. Although some scholars have studied water quality parameters such as TN, TP,  $\text{NH}_4\text{-N}$ , and  $\text{NO}_3\text{-N}$  [19,20], it is also a great challenge to estimate the concentrations of total phosphorus, total nitrogen, ammonia nitrogen, and nitrate nitrogen in inland waters because the above parameters do not have optical activity in the perception wavelength.

Based on the different platforms of the observation sensor, hyperspectral remote sensing technology can be divided into airborne, spaceborne, hand-held, and ground-based. Airborne hyperspectral remote sensing is flexible in configuration and investigation time in spatial resolution, spectral range, number of bands, and bandwidth, etc., with high spectral and spatial resolution, but limited coverage, it is more suitable for small water bodies, and continuous monitoring cannot be realized due to flight restrictions [21–23]. Spaceborne hyperspectral coverage area is higher, but the spatial and spectral resolution is relatively rough, which is not suitable for small inland water bodies. In recent decades, a series of empirical, semi-empirical, and semi-analytical algorithms have been developed to estimate water quality parameters, and Landsat, MODIS, and other methods have been used to explore long-term changes in different inland waters [24–27]. Ground-based remote sensing is a fixed point above the ground with a camera with high-resolution image acquisition and periodic image acquisition of a fixed water surface. Ground-based remote sensing can realize periodic and continuous sampling by fixing sensors on pre-planned sampling points. Under the condition of using the sun as the light source, higher spectral resolution and lower equivalent radiation noise can be obtained simultaneously. Ground-based remote sensing and proximal remote sensing have been applied to water quality testing over the last several years [28,29].

The shortage of water resources has become the main contradiction of water problems in China, especially in the northern region [30]. The northern rivers are characterized by low water volume, short flood season, long glaciation period, and high sediment content. However, previous studies have mostly focused on the southern region [31–34]. Up to date, real-time continuous monitoring of the water quality of the northern flowing, urban water streams is usually scarce, thwarting an accurate grasp of their water quality status and timely detection of water quality issues. The Haihe River is a typical river controlled by sluice in North China. The construction and operation of sluice dams change hydrological factors such as the river's flow rate and flow rate, resulting in the change of the deposition and diffusion of river pollutants and the change of water quality [35]. The ecological water of the Haihe River belongs to external water transfer, which is mainly stopped to ensure

the safety of flood control since the flood season starts in June. The aquatic species in the mainstream of the Haihe River is relatively single. The dominant population in spring every year is *Potamogeton crispus* L., which has an apparent inhibitory effect on the growth of cyanobacteria. However, the growth period of *Potamogeton crispus* L. is short, and in May, it decays and dies, and no other organisms are competing with cyanobacteria. After June, the light conditions are sufficient, and the temperature continues to rise, which is suitable for algae growth. Therefore, the end of May to early June is mostly the time when cyanobacterial outbreaks start. Tianjin is a northern region of China, and the weather has started to turn cooler by September. Therefore, May–August is the time when the Haihe River is very prone to cyanobacterial blooms. In this study, we selected stations in the Tianjin section of the Haihe River to establish ground-based hyperspectral in northern China for the first time to continuously monitor water. The relationship between reflectance spectra and water quality parameters Chl-a, PC, TSS, TN, TP, NH<sub>4</sub>-N, NO<sub>3</sub>-N, and pH was analyzed by constructing a BP machine learning model in order to use hyperspectral remote sensing fast, in real-time, and continuously, thereby understanding the water quality.

## 2. Materials and Methods

### 2.1. Study Area

The Haihe river has the comprehensive functions of drainage, storage, water supply, shipping, tourism, and environmental protection and is one of the significant water resources in Tianjin. Under the background of rapid urbanization and economic development, water shortages and water degradation have become increasingly severe in many watersheds in China [36]. In all seven river basins, the Haihe basin is suffering the most water shortages and water pollution [37]. In addition, environmental quality poses a threat to the people due to poor water quality [38]. The sampling site is located at Lishunde Wharf (89°07'15.72" N, 117°12'38.95" ), Heping District, Tianjin (Figure 1). The spectrometer is set up on the wharf, and the instrument is perpendicular to the horizontal plane, so as to avoid the influence of foreign bodies such as people walking by when it is set up on the roadside.

### 2.2. Field Data

A total of 111 samples were collected from May 2021 to August 2021. In total, 10 L of in-situ surface water (about 20 cm) was collected with a plexiglass water collector, which was stored at low temperature and brought back to the laboratory for water quality analysis as soon as possible. The water quality parameters were analyzed in the laboratory. TN, TP, NH<sub>4</sub>-N, NO<sub>3</sub>-N, TSS, and pH were measured to determine the eutrophication level of water bodies, and Chl-a and PC were used to detect cyanobacterial blooms. Water samples were filtered through 47 mm pore size GF/C membranes (Whatman) and stored to determine Chl-a and PC content. The membrane was extracted in a centrifuge tube with ethanol (4 °C, 24 h), centrifuged at 6000 rpm for 10 min, and the supernatant was obtained. The absorbance values at 630 nm, 645 nm, 663 nm, and 750 nm were measured by a UV spectrophotometer to calculate the content of Chl-a in water samples. The membrane was placed in a centrifuge tube with a 0.05 mol/L phosphate buffer, and the freeze–thaw method (freezing at −20 °C and thawing at room temperature) was repeated seven times, then the membrane was centrifuged at 12,000 rpm for 10 min, and the supernatant was obtained. The absorbance values at 615 nm and 652 nm were measured by UV spectrophotometer, and the content of PC in the water sample was calculated. The TN was measured by oxidation with potassium persulfate, and a UV spectrophotometer determined the absorbance values at 220 nm and 275 nm. TP was digested with 5% potassium persulfate for total phosphorus, molybdenum antimony anti-spectrophotometric, and the absorbance value at 700 nm was measured by UV spectrophotometer. NH<sub>4</sub>-N was measured by the Nessler reagent method, and the absorbance value at 420 nm was determined by UV spectrophotometry. NO<sub>3</sub>-N was measured by the zinc-cadmium reduction method, and the absorbance value at 543 nm was determined by UV spectrophotometry. The electrode of the pH meter was rinsed with

distilled water, immersed in the water sample, and gently shaken until the data were stable. Then the pH data were recorded.

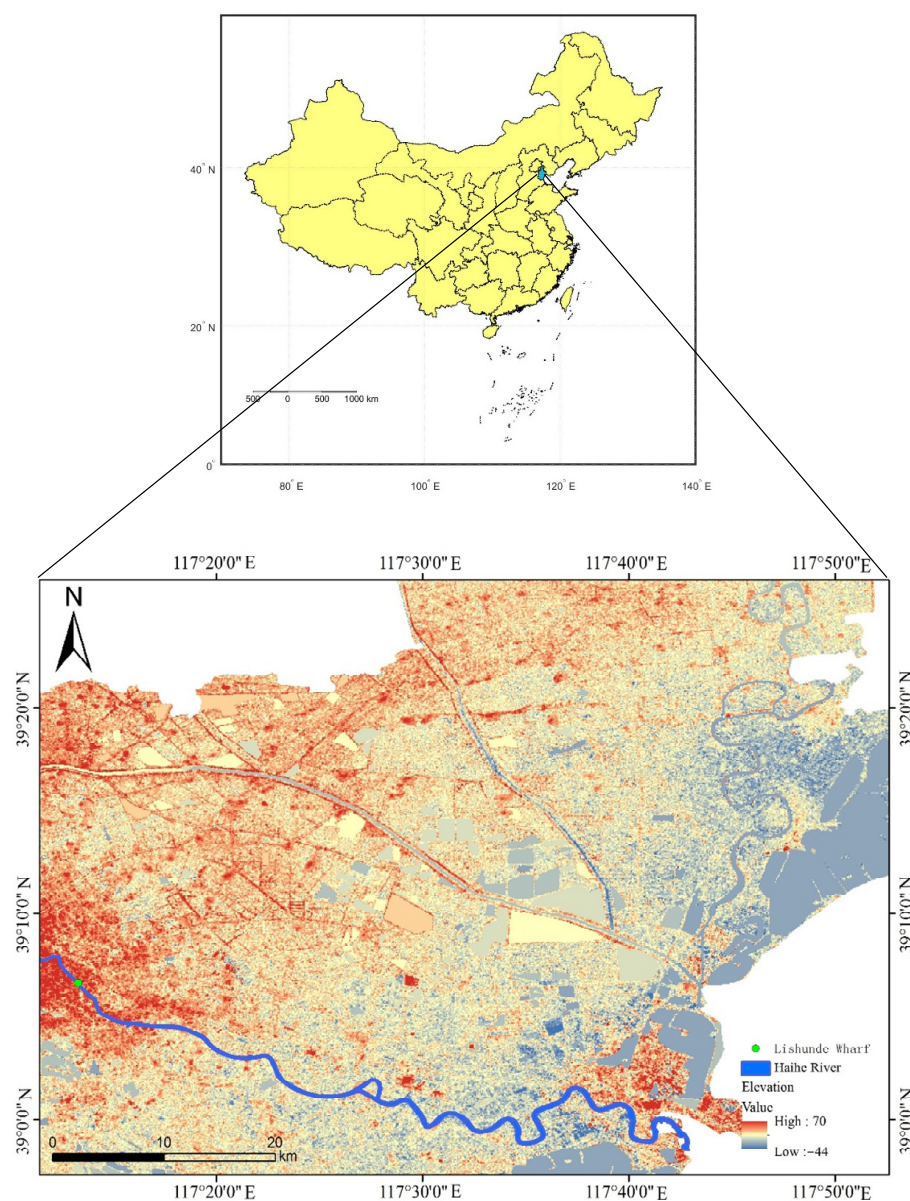


**Figure 1.** Study area map and locations of the water samples. The green dots are the sampling points of the Lishunde Wharf in the Haihe River, and the blue lines are the rivers. The highest elevation is 70 m, and the lowest is −44 m.

### 2.3. Ground-Based Hyperspectral

ATP2000P, which is a fiber optic spectrometer from Optosky Photonics Inc. in Xiamen, China, was purchased and used in this study. ATP2000P has a spectral resolution of 2.4 nm, a signal-to-noise ratio of 843:1, covering a wavelength range of 280–1130 nm, and provides 1980 spectral channels for water quality retrieval and a temporal resolution of up to the seconds level can be set according to actual needs. It can be used outdoors for a long time and can obtain spectral data remotely online. The spectrometer is approximately 3.5 m above the water surface and 0.5 m from the shore, reducing the river's bottom or riparian influence on the spectrometer, as shown in Figure 2. The measurement time ranged from 7 a.m. to 5 p.m., and the monitoring frequency was a continuous measurement with 1 min intervals.



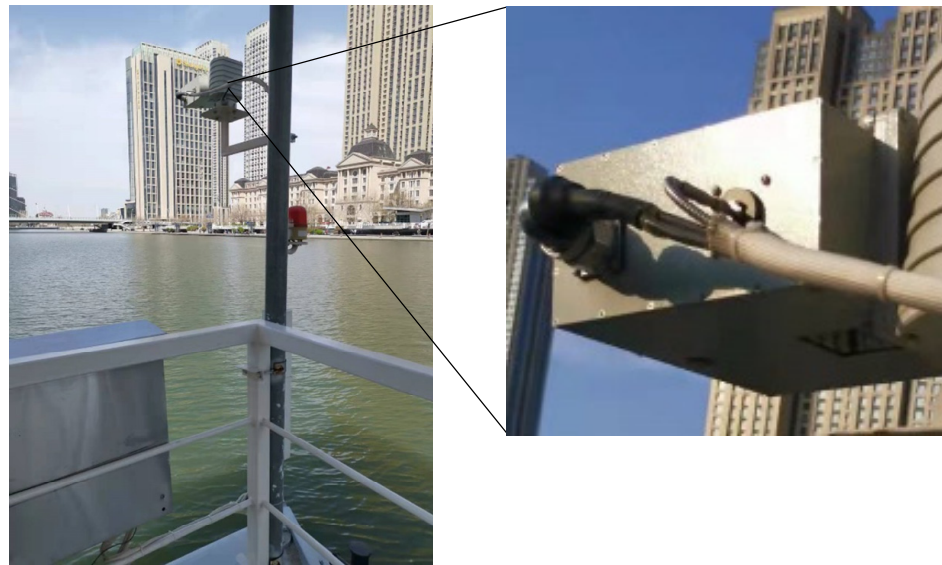


**Figure 2.** In-situ hyperspectral outdoor application system of Lishunde wharf.

Since the reflectance at the wavelength of 230–400 nm and higher than 900 nm has miscellaneous peaks, only the reflectance at 400–900 nm was retained. As the influence of shadow was caused by a different light cycle and the influence of foreign matter such as defoliation, plastic, and dead fish, the abnormal value of the water body reflectivity spectrum is higher than the normal value. The original band was screened, and the  $R_{rs}(420) \geq 20\%$  was the abnormal spectrum with a reflectivity much higher than that of the normal water spectrum, which was removed [29]. This result is shown in Figure 3.

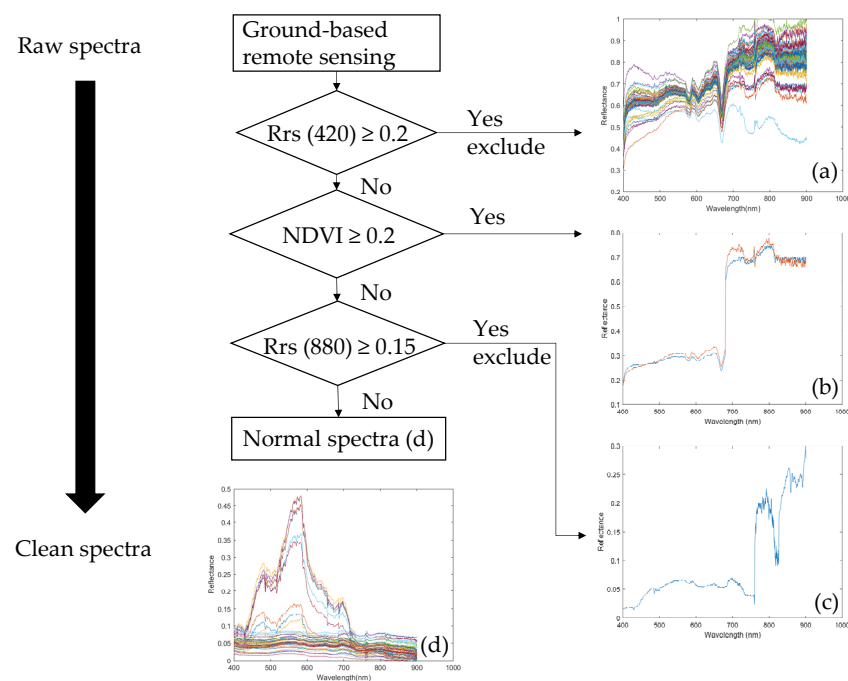


**Figure 3.** Remote sensing spectral filtering pretreatment: (a) anomalous spectra with reflectance much higher than the normal water spectrum. (b) Water surface vegetation spectra under hyperspectral imaging. (c) Hyperspectral view of anomalous floating objects on the water surface. (d) Pre-processing normal spectrum.

## 2.4. Machine Learning Models

The traditional regression model is simple and easy to operate, but it is difficult to solve complex nonlinear problems; therefore, the model inversion lacks precision [39]. In contrast, the machine learning method improves the complex relationship between independent variables and dependent variables in the process of model correction and can solve nonlinear regression problems more effectively [40].

The BP (back propagation) neural network was a concept put forward by scientists led by Rumelhart and McClelland in 1986. It is a multi-layer forward network for the weight training of nonlinear differentiable functions. It is the most widely used neural network at present. MATLAB 2019a version was used for model inversion. The input layer is the filtered spectral values, in which wavelengths of 400–900 nm for a total of 1221 input elements, and the hidden layer of 5 neuron nodes, are the best, and the output layer was set as the water quality index.

## 2.5. Accuracy Assessment

The coefficient of determination ( $R^2$ ) and root mean relative error (RMSE) for Chl-a, PC, TSS, TN, TP,  $\text{NH}_4\text{-N}$ ,  $\text{NO}_3\text{-N}$ , and pH concentrations were used to evaluate the models. Model training was mainly realized through MATLAB 2019a.

$$R^2 = 1 - \frac{\sum_i (\hat{y}_i - y_i)^2}{\sum_i (\bar{y}_i - y_i)^2} \quad (1)$$

$$\text{RMSE} = \sqrt{\frac{1}{m} \sum_{i=1}^m (\text{Meas}_i - \text{Est}_i)^2} \quad (2)$$

where  $m$  denotes the number of data points,  $i$  denotes the  $i$ th data point, and *Meas* and *Esti* denote measurements and estimates, respectively.

## 3. Results

### 3.1. Analysis of Measured Water Quality

Table 1 summarizes the measured water quality parameters in this experiment. According to the “Surface Water Environmental Quality Standard” (GB 3838-2002) in China, the index parameters were selected and displayed in Table S1. The highest value of  $\text{NH}_4\text{-N}$  exceeded the surface water class V standard, the lowest value met the requirement of water class II, and the average value met the provision of water class IV. The highest value of TN far exceeded the standard of surface water class V, the lowest value of TN met the requirement of water class III. The average value met the requirement of water class V. The highest value of TP met the requirement of water class II, and the lowest value met the provision of water class I. The average value met the requirement of water class I. Overall the water quality was below Class II. In comparison to the water quality in previous years, the overall water quality of the Haihe river tends to be better [41].

**Table 1.** Water quality parameter concentrations of Haihe Reiver.

Time	Water Quality Index	Mean $\pm$ Standard Deviation (Scope)
May to August 2021	$\text{NH}_4\text{-N}$ (mg/L)	$1.293 \pm 0.925$ (0.260–3.811)
	TN (mg/L)	$2.043 \pm 1.165$ (0.853–5.020)
	TP (mg/L)	$0.010 \pm 0.010$ (0.001–0.041)
	TSS (mg/L)	$9.311 \pm 5.370$ (2.267–25.667)
	Chl-a ( $\mu\text{g/L}$ )	$34.925 \pm 34.641$ (7.287–206.251)
	PC (mg/L)	$0.013 \pm 0.006$ (0.005–0.289)
	$\text{NO}_3\text{-N}$ (mg/L)	$3.464 \pm 2.718$ (0.728–10.594)
	pH	$7.56 \pm 0.524$ (6.06–8.19)

### 3.2. Model Development and Validation

The bands with spurious peaks below 400 nm and above 900 nm were removed first. Then, the anomalous spectra with  $R_{rs}(420) \geq 20\%$ ,  $(NIR-R)/(NIR+R) \geq 20\%$ , and  $R_{rs}(880) \geq 15\%$ , were removed from the spectra above the water. A total of 1221 bands from 400–900 nm were obtained. MATLAB 2019a was used for model construction, and the clean data, after quality control, was imported into the software. During the model construction process, input data parameters based on the Neural Network Fitting app were adjusted, 70% of the data was randomly selected for training and 30% for validating the model. The machine-learning algorithm was used to evaluate the performance of Chl-a, PC, TSS, TN, TP,  $NH_4$ -N,  $NO_3$ -N, and pH retrieval. The applicability of the models in practical applications and the errors caused by model simulations are analyzed, as shown in Figure 4 and Table 2.

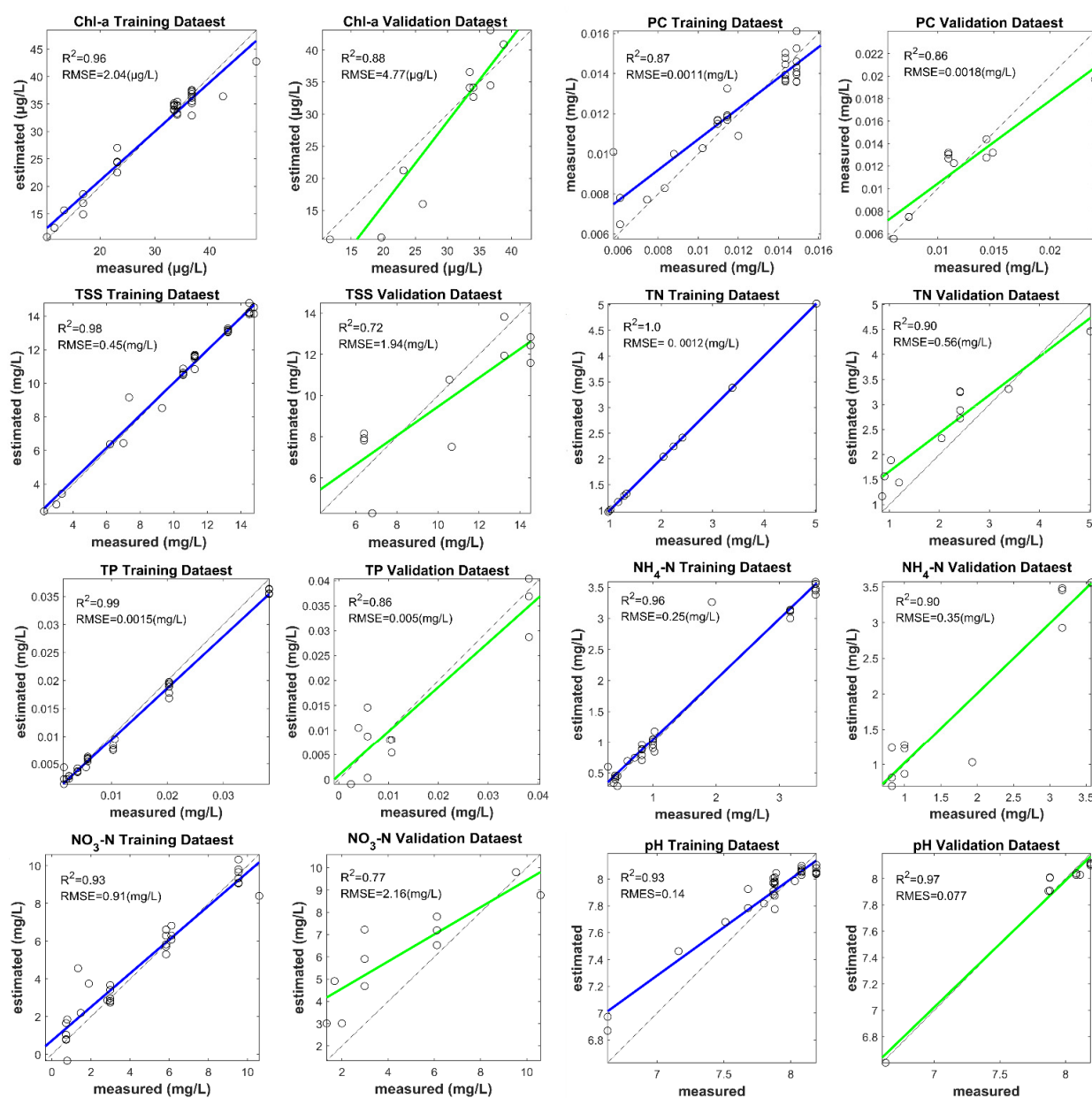


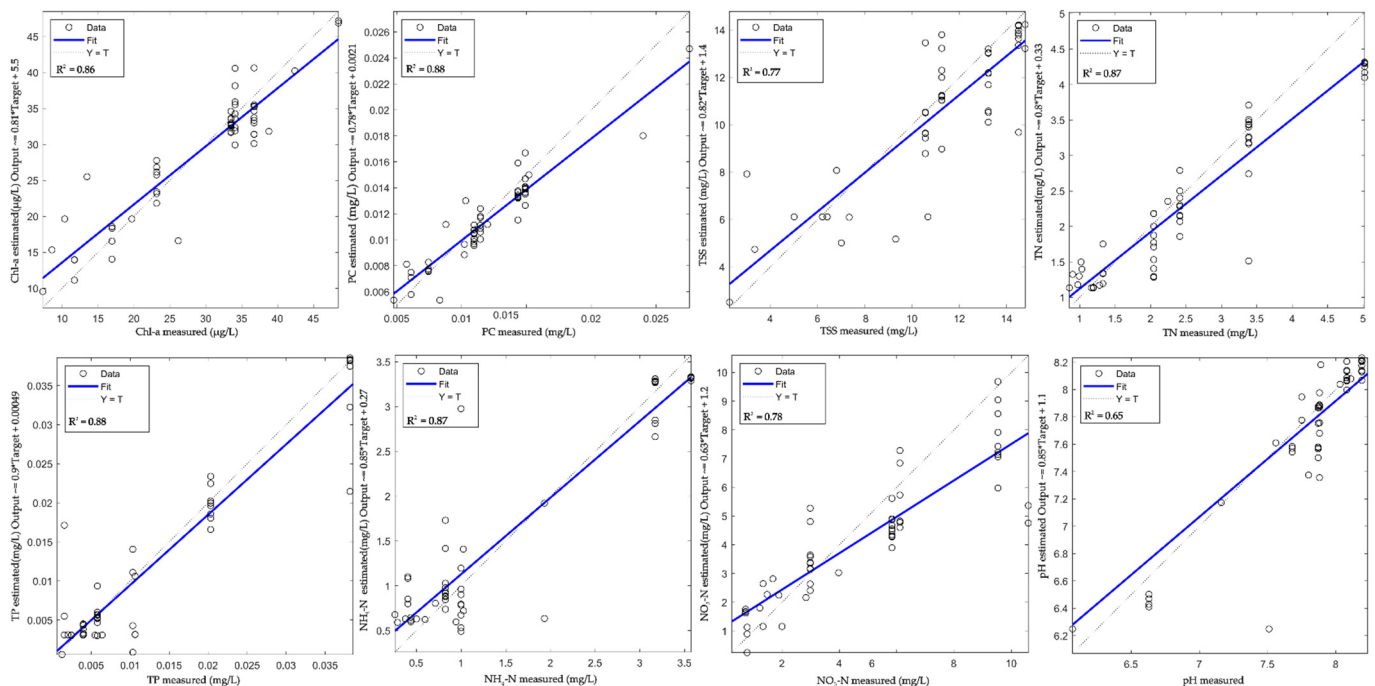
**Figure 4.** Performance evaluation of Chl-a, PC, TSS, TN, TP,  $NH_4$ -N,  $NO_3$ -N, and pH retrievals using machine-learning algorithms. The training results and the validation results of the BP neural network.

**Table 2.** Training and validation statistics ( $R^2$ , RMSE) for Chl-a, PC, TSS, TN, TP,  $\text{NH}_4\text{-N}$ ,  $\text{NO}_3\text{-N}$ , and pH concentrations based on ground-based remote sensing.

	Training Dataset		Validation Dataset	
	$R^2$	RMSE	$R^2$	RMSE
Chl-a	0.96	2.04 ( $\mu\text{g/L}$ )	0.88	4.77 ( $\mu\text{g/L}$ )
PC	0.87	0.0011 ( $\text{mg/L}$ )	0.86	0.0018 ( $\text{mg/L}$ )
TSS	0.98	0.45 ( $\text{mg/L}$ )	0.72	1.94 ( $\text{mg/L}$ )
TN	1.0	0.0012 ( $\text{mg/L}$ )	0.90	0.056 ( $\text{mg/L}$ )
TP	0.99	0.0015 ( $\text{mg/L}$ )	0.86	0.005 ( $\text{mg/L}$ )
$\text{NH}_4\text{-N}$	0.96	0.25 ( $\text{mg/L}$ )	0.90	0.35 ( $\text{mg/L}$ )
$\text{NO}_3\text{-N}$	0.93	0.91 ( $\text{mg/L}$ )	0.77	2.16 ( $\text{mg/L}$ )
pH	0.93	0.14	0.97	0.077

The machine learning model performance of all water quality in this experiment was good ( $R^2 \geq 0.72$ ). The model training results show that the coefficient of determination of Chl-a, TSS, TN, TP,  $\text{NH}_4\text{-N}$ ,  $\text{NO}_3\text{-N}$ , and pH are all  $R^2 > 0.9$ , being better than that of PC, which was  $R^2 = 0.87$ . The model verification results show that TSS and  $\text{NO}_3\text{-N}$  content estimation models are low. The coefficient of determination of TSS and  $\text{NO}_3\text{-N}$  are  $R^2 < 0.8$ . The coefficient of determination of Chl-a, TN, TP,  $\text{NH}_4\text{-N}$ , and PC are  $R^2 > 0.8$ .

To further analyze the applicability of models in practical application and the error caused by model simulation, the measured data and model simulation data of all sampling points were selected for linear fitting, as shown in Figure 5. The results show that an accuracy of over 70% for TSS ( $R^2 = 0.77$ ),  $\text{NO}_3\text{-N}$  ( $R^2 = 0.78$ ), and over 80% for Chl-a ( $R^2 = 0.86$ ), PC ( $R^2 = 0.88$ ), TN ( $R^2 = 0.87$ ), TN ( $R^2 = 0.88$ ), and  $\text{NH}_4\text{-N}$  ( $R^2 = 0.87$ ). Only pH ( $R^2 = 0.65$ ) was over 60%.

**Figure 5.** The measured data and model simulation data of all sampling points were selected for linear fitting.

#### 4. Discussion

Widespread water pollution in China poses a serious challenge to sustainable social and economic development and the improvement of people's livelihoods [42]. The 2015



Annual Report on China's Environmental Quality released by the Ministry of Environmental Protection, according to Five Classes of Water Bodies Specified in Chinese Surface Water Quality Standard (GB3838-2002), the water quality of the mainstream of the Haihe River is in class V and worse than Class V [43]. In contrast, water quality ranged from Class III to Class V on some dates during the experimental phase. In recent years, the state attaches great importance to the water environment, and the water quality of the mainstream of Haihe river has been improved to a certain extent. The adverse effects of the construction of the sluice and dam on the water body make it difficult to study the changing characteristics of the water quality and the water environment control of the Northern Rivers. Hyperspectral remote sensing offers new options for water environmental monitoring. There are several problems in the high precision remote sensing estimation of inland water quality parameters. First, existing spaceborne hyperspectral sensors are more suitable for large-scale water and land, such as the Landsat, MODIS, and Gaofen series launched by China. Second, the complex optical characteristics increase the difficulty of remote sensing inland waters. Most previous studies concentrate mainly on monitoring the substances with optical properties in the water, such as chlorophyll [44–46] and CDOM [47]. Relatively few studies focused on components that lack optical properties in the water, e.g., TN, TP,  $\text{NH}_4\text{-N}$ , and  $\text{NO}_3\text{-N}$  [20]. This made it difficult to construct a higher precision remote sensing model. Thirdly, cyanobacteria and vertical movement is driven by gas vesicles which lead to their vertical distribution in water being uneven. The signals obtained by remote sensing are only surface water and the quantitative inversion model is challenging to represent various heterogeneity characteristics of cyanobacteria blooms effectively. So it may not be easy to obtain accurate information on chlorophyll concentrations [48]. The biggest advantage of ground remote sensing is that it can achieve continuous monitoring with high Spatio-temporal resolution and high spectral resolution (2.4 nm). Besides, the device can be fixed beside any water body that needs to be monitored with simple support, not only limited to rivers and lakes, but also aquaculture water bodies, sewage treatment inlet, and outlet, which can be used in multiple scenarios. As the hyperspectral probe is close to the water surface, there is no need for complex atmospheric correction, and the correction can be automatically performed each time the data is collected. Moreover, a trained water quality parameter estimation algorithm can be embedded in the hyperspectral imaging system to display the water quality parameter concentration in real-time while preserving the spectral information so as to help decision-makers fully understand the real-time changes of water quality. Therefore, the installation of ground-based hyperspectral remote sensing in the mainstream of the Haihe River is of great practical significance for the continuous monitoring of the water quality in the Haihe River.

In recent years, hyperspectral technology has become increasingly mature. Several linear regression empirical models using single band and single band ratios have been established. The empirical model has the advantages of a fast data processing speed and simple modeling. Still, when the established model is applied to other water bodies with different concentrations or different types of optically active components, the model is not applicable [49–51]. The bio-optical model is also a common method for inversion of water quality parameters of inland water, which needs to consider various water quality conditions [52]. This study builds the BP neural network models based on the solid nonlinear mapping capability, the high self-learning and self-adaptive capability, and the fault tolerance capability. The system usually works even in case of localized damage and therefore has high robustness. In our study, the BP machine learning model showed high  $R^2$  values when fitted. We evaluated both the training and testing set to verify that our predictive model and select the optimal results of each model. The model with the highest fitting degree was TN ( $R^2 = 1$ , RMSE = 0.0012 mg/L), which was much higher than that of the Sun et al. BP neural network model ( $R^2 = 0.83$ , RMSE = 0.23 mg/L) [29] and the Song et al. Ga-pls model ( $R^2 = 0.88$ , RMSE = 0.07 mg/L) [53]. This may be due to the limited amount of data that resulted in over-fitting. An overall accuracy of over 90% for our result of TP ( $R^2 = 0.99$ , RMSE = 0.0015 mg/L), Sun's result of TP ( $R^2 = 0.93$ , RMSE = 0.02 mg/L),

and Song's result of TP ( $R^2 = 0.91$ , RMSE = 0.017 mg/L), was found. Among our results, the lowest fitting degree was PC ( $R^2 = 0.87$ , RMSE = 0.0011 mg/L), with results a little more than Pyo et al.'s SAE-ANN model ( $R^2 = 0.82$ , RMSE = 9.32 mg/L) [13]. The retrieval of the Chl-a concentration has always been the focus of water color remote sensing research. Monitoring Chl-a concentration in inland water has become the frontier of watercolor remote sensing worldwide [54]. Our value of Chl-a ( $R^2 = 0.96$ , RMSE = 2.04  $\mu\text{g/L}$ ), indicates an excellent fit. Model inversion of TSS has been proposed as a hot spot in remote sensing research for several years. In the present study, we generated a robust BP neural network to predict TSS with a reflectance spectrum. The result indicates a strong correlation between them with  $R^2 = 0.98$ . Higher than Jensen et al., the VIP-filtered first derivative-based PLSR model attained an  $R^2$  of 0.83 [55]. The training model of  $\text{NO}_3\text{-N}$  showed a good fitting  $R^2 = 0.93$  and RMSE = 0.91 mg/L, but the fitting of the validation model was significantly lower than that of the training model, showing  $R^2 = 0.77$  and RMSE = 2.16 mg/L. In this study, while the BP neural network shows a good fit, it also exposes the model's limitations. Most obviously, the model solves a complex nonlinearization problem in which the network's weights are adjusted gradually by moving along the direction of local improvement, which can cause the algorithm to fall into local extremes and cause local miniaturization problems. In turn, it has been found that the learning rate of the BP network is not stable enough, and there may be a situation where the results obtained from multiple training sessions are different.

At present, the sampling time of this experiment is mainly concentrated in May to August, the amount of data collected is limited, and the results are limited to the concentration range of each water parameter. In addition, the northern water body is characterized by freezing in winter. It is still uncertain whether the BP neural network model constructed in this study applies to other seasons in the Haihe River. It is necessary to continue collecting data from additional months in the subsequent research to fit the model further so that it applies to all months except the icing period. In the future, the inversion model will be input into the hyperspectral remote sensing system so as to achieve the overall monitoring of annual changes in water quality of the mainstream of the Haihe River. At present, the range of concentration variation of accumulated water quality parameters is limited, and there is great uncertainty in extrapolating the established model algorithm to other waters with lower or higher concentrations. In the future, more different water will be accumulated: black-odor water, clean water, breeding water, etc., to increase the amount of data, optimize the algorithm, and improve the adaptability of the model in different water bodies. Future studies will also explore the use of more machine learning models, such as deep learning. Water resources affect the survival and development of human beings. In the course of social and economic development, the water resources are seriously affected, and the water environment deteriorates. As a developing country, China's natural environment has undergone great changes in recent decades [56,57]. Therefore, the monitoring of the water environment is particularly important. The remote sensing sensor has the characteristics of large-scale and dynamic observation and can quickly obtain a broad-spectrum of information for a water area. Various water quality parameters can be obtained through data modeling and retrieval. Therefore, remote sensing has gradually become an indispensable means of water environment monitoring. With the development of technology and practical needs, satellite, UAV, and ground remote sensing can be combined to build an integrated monitoring system of satellite, UAV, and ground-based remote sensing. Satellite remote sensing pictures of different bands can be combined with ground-based synchronous measured data to achieve joint monitoring between heaven and earth. The foundation of a water quality automatic online monitoring system can meet the requirements of daily tracking to perform considerable time and space scale continuous monitoring. When combined with space-based satellite images, one can quickly discern traces of the sources of pollution with timeliness and convenience. This has the ability to provide timely warnings, assessments, and emergency relief for the integrated prevention and control of environmental pollution, ecological changes, disaster monitoring, etc.

## 5. Conclusions

Our results show the ground-based remote sensing technology for water quality (Chl-a, PC, TSS, TN, TP, NH<sub>4</sub>-N, NO<sub>3</sub>-N and pH) monitoring of the river in North China and demonstrate their feasibility based on field observation. Ground-based remote sensing combined with a BP neural network has great potential in the estimation of water quality parameters of inland waters. The determination coefficients  $R^2$  of Chl-a, PC, TSS, TP, TN, NH<sub>4</sub>-N, NO<sub>3</sub>-N, and pH were all above 0.8, and the monitoring results were accurate. The validation results showed that the determination coefficients  $R^2$  of Chl-a, PC, TN, TP, NH<sub>4</sub>-N, NO<sub>3</sub>-N, and pH were all above 0.8, and the determination coefficients of TTS were above 0.7. Ground-based remote sensing realizes continuous observation with high spatio-temporal resolution and high spectral resolution (2.4 nm), providing an effective and practical method for the long-term continuous monitoring of the inland water quality of rivers, lakes, reservoirs, and aquaculture water. In future studies, the water samples obtained during different months of the year from the Haihe River, and more water samples and water quality parameters of inland waters in various environments, will be continuously collected to improve the robustness of the models in combination with satellite, UAV, and ground-based remote sensing to achieve the integration of online water quality monitoring and early warning systems. Furthermore, the water samples and water quality parameters of the aquaculture water environment will be collected to promote the application of ground-based remote sensing in the aquaculture water environment.

**Supplementary Materials:** The following supporting information can be downloaded at: <https://www.mdpi.com/article/10.3390/w14010022/s1>, Table S1: Surface water environmental quality standards part of the project standard limits

**Author Contributions:** All authors contributed significantly to the preparation of this manuscript. Conceptualization, Q.C.; methodology, Q.C., G.Y. and S.S.; software, Q.C., S.S. and Y.D.; formal analysis, Q.C.; investigation, Q.C. and G.Y.; resources, Q.C.; data curation, Q.C. and Z.Q.; writing—original, Q.C.; writing—review and editing, G.Y., Y.D., H.L. and Z.Q.; visualization, Q.C. and Z.Q.; supervision, Z.Q.; project administration, Z.Q. and G.Y.; funding acquisition, Z.Q. All authors have read and agreed to the published version of the manuscript.

**Funding:** This research was funded by a Major Project of Ecological Environment Management in Tianjin (Grant No. 18ZXSZSF00080), the National Key Research and Development Program of China (Grant No. 2017YFA0605201), and the National Natural Science Foundation of China (Grant No. 51779247).

**Institutional Review Board Statement:** Not applicable.

**Informed Consent Statement:** Not applicable.

**Data Availability Statement:** Not applicable.

**Acknowledgments:** We would like to thank all colleagues for participating in on-site sample collection and chemical analysis, especially Xijun Yang, Zihao Sun, Yuan Gao, and Can Wang. We would like to express our deep appreciation to Da Huo for his constructive suggestions in the manuscript. The modelling processes was powered and supported by the Wuhan Branch, Supercomputing Center, Chinese Academy of Sciences, China.

**Conflicts of Interest:** The authors declare no conflict of interest.

## References

1. Liying, L. Assessment of water resource security in karst area of Guizhou Province, China. *Sci. Rep.* **2021**, *11*, 7641. [\[CrossRef\]](#)
2. Salem, S.I.; Higa, H.; Kim, H.; Kobayashi, H.; Oki, K.; Oki, T. Assessment of Chlorophyll-a Algorithms Considering Different Trophic Statuses and Optimal Bands. *Sensors* **2017**, *17*, 1746. [\[CrossRef\]](#)
3. Mackay, E.B.; Feuchtmayr, H.; De Ville, M.M.; Thackeray, S.J.; Callaghan, N.; Marshall, M.; Rhodes, G.; Yates, C.A.; Johnes, P.J.; Maberly, S.C. Dissolved organic nutrient uptake by riverine phytoplankton varies along a gradient of nutrient enrichment. *Sci. Total Environ.* **2020**, *722*, 137837–137851. [\[CrossRef\]](#)
4. Duan, W.L.; He, B.; Takara, K.; Luo, P.P.; Nover, D.; Sahu, N.; Yamashiki, Y. Spatiotemporal evaluation of water quality incidents in Japan between 1996 and 2007. *Chemosphere* **2013**, *93*, 946–953. [\[CrossRef\]](#)

5. Wan, W.; Long, D.; Hong, Y.; Ma, Y.; Yuan, Y.; Xiao, P.; Duan, H.; Han, Z.; Gu, X. A lake data set for the Tibetan Plateau from the 1960s, 2005, and 2014. *Sci. Data* **2016**, *3*, 160039–160052. [\[CrossRef\]](#)
6. Khan, M.J.; Khan, H.S.; Yousaf, A.; Khurshid, K.; Abbas, A. Modern Trends in Hyperspectral Image Analysis: A Review. *IEEE Access* **2018**, *6*, 14118–14129. [\[CrossRef\]](#)
7. Landgrebe, D. Hyperspectral image data analysis. *IEEE Signal Process. Mag.* **2002**, *19*, 17–28. [\[CrossRef\]](#)
8. Krutz, D.; Muller, R.; Knodt, U.; Gunther, B.; Walter, I.; Sebastian, I.; Sauberlich, T.; Reulke, R.; Carmona, E.; Eckardt, A.; et al. The Instrument Design of the DLR Earth Sensing Imaging Spectrometer (DESI). *Sensors* **2019**, *19*, 1622. [\[CrossRef\]](#)
9. Zhang, Y.; Qin, B.; Chen, W. Advances and main applications of lake optics research. *Chin. J. Oceanol. Limnol.* **2005**, *23*, 284–290.
10. Yi, X.; Xuan-yan, D.; Jun-jie, W. Use of Remote Multispectral Imaging to Monitor Chlorophyll-a in Taihu Lake: A Comparison of Four Machine Learning Models. *J. Hydroecol.* **2019**, *40*, 48–57.
11. Pahlevan, N.; Smith, B.; Schalles, J.; Binding, C.; Cao, Z.; Ma, R.; Alikas, K.; Kangro, K.; Gurlin, D.; Hà, N.; et al. Seamless retrievals of chlorophyll-a from Sentinel-2 (MSI) and Sentinel-3 (OLCI) in inland and coastal waters: A machine-learning approach. *Remote Sens. Environ.* **2020**, *240*, 111604. [\[CrossRef\]](#)
12. Sun, D.; Li, Y.; Wang, Q.; Gao, J.; Le, C.; Huang, C.; Gong, S. Hyperspectral Remote Sensing of the Pigment C-Phycocyanin in Turbid Inland Waters, Based on Optical Classification. *IEEE Trans. Geosci. Remote Sens.* **2013**, *51*, 3871–3884. [\[CrossRef\]](#)
13. Pyo, J.; Duan, H.; Ligaray, M.; Kim, M.; Baek, S.; Kwon, Y.S.; Lee, H.; Kang, T.; Kim, K.; Cha, Y.; et al. An Integrative Remote Sensing Application of Stacked Autoencoder for Atmospheric Correction and Cyanobacteria Estimation Using Hyperspectral Imagery. *Remote Sens.* **2020**, *12*, 1073. [\[CrossRef\]](#)
14. Uudeberg, K.; Aavaste, A.; Kõks, K.-L.; Ansper, A.; Uusõue, M.; Kangro, K.; Ansko, I.; Ligi, M.; Toming, K.; Reinart, A. Optical Water Type Guided Approach to Estimate Optical Water Quality Parameters. *Remote Sens.* **2020**, *12*, 931. [\[CrossRef\]](#)
15. Zhen, Y.; Xiaoping, L.; Yongbin, W.; Peiji, M.; Junli, Z. Retrieval and model construction of water quality parameters for UAV hyperspectral remote sensing. *Sci. Surv. Mapp.* **2020**, *45*, 60–64, 95.
16. Arabi, B.; Salama, M.S.; Pitarch, J.; Verhoef, W. Integration of in-situ and multi-sensor satellite observations for long-term water quality monitoring in coastal areas. *Remote. Sens. Environ.* **2020**, *239*, 111632. [\[CrossRef\]](#)
17. Wang, Z.; Huang, C.; Zhang, Y.; Wang, Z.; Xia, H.; Cao, L. Transparency Estimation of Narrow Rivers by UAV-Borne Hyperspectral Remote Sensing Imagery. *IEEE Access* **2020**, *8*, 168137–168153. [\[CrossRef\]](#)
18. Legleiter, C.J.; Paul, I.I.; Erwin, S.O.; Bulliner, E.A. An Experimental Evaluation of the Feasibility of Inferring Concentrations of a Visible Tracer Dye from Remotely Sensed Data in Turbid Rivers. *Remote. Sens.* **2019**, *12*, 57. [\[CrossRef\]](#)
19. Qun'ou, J.; Lidan, X.; Siyang, S.; Meilin, W.; Huijie, X. Retrieval model for total nitrogen concentration based on UAV hyperspectral remote sensing data and machine learning algorithms—A case study in the Miyun Reservoir, China. *Ecol. Indic.* **2021**, *124*, 107356. [\[CrossRef\]](#)
20. Al-Shaibah, B.; Liu, X.; Zhang, J.; Tong, Z.; Zhang, M.; El-Zeiny, A.; Faichia, C.; Hussain, M.; Tayyab, M. Modeling Water Quality Parameters Using Landsat Multispectral Images: A Case Study of Erlong Lake, Northeast China. *Remote Sens.* **2021**, *13*, 1603. [\[CrossRef\]](#)
21. Niu, C.; Tan, K.; Jia, X.; Wang, X. Deep learning based regression for optically inactive inland water quality parameter estimation using airborne hyperspectral imagery. *Environ. Pollut.* **2021**, *286*, 117534. [\[CrossRef\]](#)
22. Guild, L.S.; Kudela, R.M.; Hooker, S.B.; Palacios, S.L.; Houskeeper, H.F. Airborne Radiometry for Calibration, Validation, and Research in Oceanic, Coastal, and Inland Waters. *Front. Environ. Sci.* **2020**, *8*, 585529. [\[CrossRef\]](#)
23. Yim, I.; Shin, J.; Lee, H.; Park, S.; Nam, G.; Kang, T.; Cho, K.H.; Cha, Y. Deep learning-based retrieval of cyanobacteria pigment in inland water for in-situ and airborne hyperspectral data. *Ecol. Indic.* **2020**, *110*, 105879. [\[CrossRef\]](#)
24. Yang, H.; Shuanggen, J.; Wei, S. Water Quality Variability and Related Factors along the Yangtze River Using Landsat-8. *Remote Sensing* **2021**, *13*, 2241. [\[CrossRef\]](#)
25. Hunter, P.D.; Tyler, A.N.; Carvalho, L.; Codd, G.A.; Maberly, S.C. Hyperspectral remote sensing of cyanobacterial pigments as indicators for cell populations and toxins in eutrophic lakes. *Remote Sens. Environ.* **2010**, *114*, 2705–2718. [\[CrossRef\]](#)
26. Feng, L.; Xinyan, L.; Foody, M.G.; Doreen, B.; Yong, G.; Xiaodong, L.; Yun, D. Monitoring surface water area variations of reservoirs using daily MODIS images by exploring sub-pixel information. *ISPRS J. Photogramm. Remote Sens.* **2020**, *168*, 141–152. [\[CrossRef\]](#)
27. Luo, J.; Pu, R.; Ma, R.; Wang, X.; Lai, X.; Mao, Z.; Zhang, L.; Peng, Z.; Sun, Z. Mapping Long-Term Spatiotemporal Dynamics of Pen Aquaculture in a Shallow Lake: Less Aquaculture Coming along Better Water Quality. *Remote Sens.* **2020**, *12*, 1866. [\[CrossRef\]](#)
28. Liew, S.C.; Choo, C.K.; Lau, J.; Chan, W.S.; Dang, T.C. Monitoring water quality in Singapore reservoirs with hyperspectral remote sensing technology. *Water Pract. Technol.* **2019**, *14*, 118–125. [\[CrossRef\]](#)
29. Sun, X.; Zhang, Y.; Shi, K.; Zhang, Y.; Li, N.; Wang, W.; Huang, X.; Qin, B. Monitoring water quality using proximal remote sensing technology. *Sci. Total Environ.* **2021**, *803*, 149805. [\[CrossRef\]](#)
30. Qiu, Y.; Liu, Y.; Liu, Y.; Chen, Y.; Li, Y. An Interval Two-Stage Stochastic Programming Model for Flood Resources Allocation under Ecological Benefits as a Constraint Combined with Ecological Compensation Concept. *Int. J. Environ. Res. Public Health* **2019**, *16*, 1033. [\[CrossRef\]](#)
31. Lei, F.; Yu, Y.; Zhang, D.; Feng, L.; Guo, J.; Zhang, Y.; Fang, F.; Maseleno, A.; Yuan, X.; Balas, V.E. Water remote sensing eutrophication inversion algorithm based on multilayer convolutional neural network. *J. Intell. Fuzzy Syst.* **2020**, *39*, 5319–5327. [\[CrossRef\]](#)



32. Zhang, B.; Shen, Q.; Li, J.; Zhang, H.; Wu, D. Retrieval of three kinds of representative water quality parameters of Lake Taihu from hyperspectral remote sensing data. *J. Lake Sci.* **2009**, *21*, 182–192.
33. Lin, J.; Zhang, C. Inversion of Water Quality Parameters of Urban River Network Using Airborne Hyperspectral Remote Sensing. *Remote Sens. Inf.* **2019**, *34*, 23–29.
34. Xiao, L.; PuZe, W.; ManTang, X.; Shao-Wen, Y.; Tang-Lin, Z.; Jia-Shou, L.; Zhong-Jie, L. Study on the spatiotemporal dynamics of water quality in Lake Longgan based on principle component analysis (PCA) and self-organizing mapping neural network (SOM) modelling. *Acta Hydrobiol. Sin.* **2021**, *45*, 1104–1111.
35. Domingues, R.B.; Barbosa, A.B.; Sommer, U.; Galvao, H.M. Phytoplankton composition, growth and production in the Guadiana estuary (SW Iberia): Unraveling changes induced after dam construction. *Sci. Total Environ.* **2012**, *416*, 300–313. [[CrossRef](#)]
36. Zong, M.; Hu, Y.; Liu, M.; Li, C.; Wang, C.; Ping, X. Effects of Landscape Pattern Change on Water Yield and Nonpoint Source Pollution in the Hun-Taizi River Watershed, China. *Int. J. Environ. Res. Public Health* **2020**, *17*, 3060. [[CrossRef](#)]
37. Feng, A.; Wang, X.; Xu, Y.; Li, H.; Chuan-qing, W. Assessment of Potential Risk of Diffuse Pollution in Haihe River Basin Based Using DPERS Model. *Environ. Sci.* **2020**, *41*, 4555–4563. [[CrossRef](#)]
38. Chen, X.; Chen, W.; Bai, Y.; Wen, X. Changes in turbidity and human activities along Haihe River Basin during lockdown of COVID-19 using satellite data. *Environ. Sci. Pollut. Res. Int.* **2021**. [[CrossRef](#)]
39. Zhang, Y.; Qian, X.; Qian, Y.; Liu, J.; Kong, F. Application of SVM on Chl-a concentration retrievals in Taihu Lake. *China Environ. Sci.* **2009**, *29*, 78–83.
40. Lary, D.J.; Alavi, A.H.; Gandomi, A.H.; Walker, A.L. Machine learning in geosciences and remote sensing. *Geoenviron. Front.* **2016**, *7*, 3–10. [[CrossRef](#)]
41. Yu, Z.; Yonghui, S.; Jian, W.; Shugang, H.; Qiu, J. 70 Years' Governance Process of Haihe River. *Res. Environ. Sci.* **2021**, *34*, 1347–1358. [[CrossRef](#)]
42. Han, D.; Currell, M.J.; Cao, G. Deep challenges for China's war on water pollution. *Environ. Pollut.* **2016**, *218*, 1222–1233. [[CrossRef](#)] [[PubMed](#)]
43. Yang, X.; Liu, Q.; Luo, X.; Zheng, Z. Spatial Regression and Prediction of Water Quality in a Watershed with Complex Pollution Sources. *Sci. Rep.* **2017**, *7*, 8318. [[CrossRef](#)] [[PubMed](#)]
44. Zhang, Y.; Hallikainen, M.; Zhang, H.; Duan, H.; Li, Y.; Liang, X.S. Chlorophyll-a Estimation in Turbid Waters Using Combined SAR Data With Hyperspectral Reflectance Data: A Case Study in Lake Taihu, China. *IEEE J. Sel. Top. Appl. Earth Obs. Remote Sens.* **2018**, *11*, 1325–1336. [[CrossRef](#)]
45. Lai, Y.; Zhang, J.; Song, Y.; Gong, Z. Retrieval and Evaluation of Chlorophyll-a Concentration in Reservoirs with Main Water Supply Function in Beijing, China, Based on Landsat Satellite Images. *Int. J. Environ. Res. Public Health* **2021**, *18*, 4419. [[CrossRef](#)]
46. Silveira Kupssinsku, L.; Thomassim Guimaraes, T.; Menezes de Souza, E.; Zanotta, D.C.; Roberto Veronez, M.; Gonzaga, L., Jr.; Mauad, F.F. A Method for Chlorophyll-a and Suspended Solids Prediction through Remote Sensing and Machine Learning. *Sensors* **2020**, *20*, 2125. [[CrossRef](#)]
47. Zhang, Y.; Zhou, L.; Zhou, Y.; Zhang, L.; Yao, X.; Shi, K.; Jeppesen, E.; Yu, Q.; Zhu, W. Chromophoric dissolved organic matter in inland waters: Present knowledge and future challenges. *Sci. Total Environ.* **2021**, *759*, 143550. [[CrossRef](#)]
48. Lian, F. Key issues in detecting lacustrine cyanobacterial bloom using satellite remote sensing. *J. Lake Sci.* **2021**, *33*, 647–652. [[CrossRef](#)]
49. McCullough, I.M.; Loftin, C.S.; Sader, S.A. Combining lake and watershed characteristics with Landsat TM data for remote estimation of regional lake clarity. *Remote Sens. Environ.* **2012**, *123*, 109–115. [[CrossRef](#)]
50. Yang, W.; Matsushita, B.; Chen, J.; Fukushima, T. Estimating constituent concentrations in case II waters from MERIS satellite data by semi-analytical model optimizing and look-up tables. *Remote Sens. Environ.* **2011**, *115*, 1247–1259. [[CrossRef](#)]
51. Hong-Tao, D.; Bai, Z.; Kai-Shan, S.; Zong-Ming, W. Evaluation of Secchi Disk Transparency by Using Field Spectral Measurements in Nanhu Lake, Changchun. *J. Grad. Sch. Chin. Acad. Sci.* **2006**, *23*, 633–639.
52. Duan, H.; Ma, R.; Hu, C. Evaluation of remote sensing algorithms for cyanobacterial pigment retrievals during spring bloom formation in several lakes of East China. *Remote Sens. Environ.* **2012**, *126*, 126–135. [[CrossRef](#)]
53. Song, K.; Li, L.; Tedesco, L.; Li, S.; Shi, K.; Hall, B. Remote Estimation of Nutrients for a Drinking Water Source Through Adaptive Modeling. *Water Resour. Manag.* **2014**, *28*, 2563–2581. [[CrossRef](#)]
54. Bing, Z.; Junsheng, L.; Qian, S.; Yanhong, W.; Fangfang, Z.; Shenglei, W.; Yue, Y.; GUOLinan; Ziyao, Y. Recent research progress on long time series and large scale optical remote sensing of inland water. *Natl. Remote Sens. Bull.* **2021**, *25*, 37–52.
55. Jensen, D.; Simard, M.; Cavanaugh, K.; Sheng, Y.; Twilley, R. Improving the Transferability of Suspended Solid Estimation in Wetland and Deltaic Waters with an Empirical Hyperspectral Approach. *Remote Sens.* **2019**, *11*, 1629–1653. [[CrossRef](#)]
56. Jing, T. Water Quality Monitoring and Standardization in China: A Review. *IOP Conf. Ser. Earth Environ. Sci.* **2020**, *546*, 032050. [[CrossRef](#)]
57. Da, H.; Nanqin, G.; Ruozhen, G.; Qi, C.; Song, L.; Yu, G.; Li, R. Cyanobacterial blooms in China: Diversity, distribution, and cyanotoxins. *Harmful Algae* **2020**, *109*, 102106. [[CrossRef](#)]